Transport of Spin-Entangled Triplet Excitons Generated by Singlet Fission

Yan Wan[1,2], Gary P. Wiederrecht[3], Richard D. Schaller[3,4], Justin C. Johnson[5], and Libai Huang[2*]

[1] College of Chemistry, Beijing Normal University, Beijing 100875, China

[2] Department of Chemistry, Purdue University, West Lafayette, IN 47907, USA

[3] Center for Nanoscale Materials, Argonne National Laboratory, Argonne, IL 60439, USA

[4] Department of Chemistry, Northwestern University, Evanston, IL 60208, USA

[5] National Renewable Energy Laboratory, 15013 Denver West Pkwy, Golden, CO 80401, USA

[*]Corresponding author; Email: libai-huang@purdue.edu

Abstract

Singlet fission provides a promising route for overcoming the Shockley-Queisser limit in solar cells using organic materials. Despite singlet fission dynamics have been extensively investigated, the transport of the various intermediates in relation to the singlet and triplet states is largely unknown. Here we employ temperature-dependent ultrafast transient absorption microscopy to image the transport of singlet fission intermediates in single crystals of tetracene. These measurements suggest a mobile singlet fission intermediate state at low temperatures, with a diffusion constant of 36 cm^2s^{-1} at 5 K, approaching that for the free singlet excitons, which we attribute to the spin-entangled correlated triplet pair state ^{1}[TT]. These results indicate that ^{1}[TT] could transport with a similar mechanism as the bright singlet excitons, which has important implications in designing materials for singlet fission and spintronic applications.

TOC:

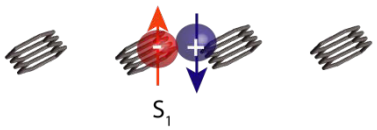

S_1

$D_s = 52\ cm^2s^{-1}$ (5 K)

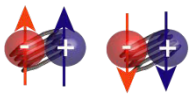

$^1[TT]$

$D_{TT} = 36\ cm^2s^{-1}$ (5 K)

Singlet fission, in which an excited singlet state shares its excitation energy with a neighboring ground-state chromophore and both are converted into triplet-excited states,[1] is promising for overcoming the Shockley-Queisser limit in solar cells.[2] The generally accepted mechanism of singlet fission in polyacene crystals is postulated to involve a doubly-excited singlet state ^{1}[TT] as an intermediate state, also known as the multi-exciton state[3-7] as schematically shown in Fig.1. In a molecular crystal, ^{1}[TT] can separate physically by triplet−triplet energy transfer to form a spatially separated yet spin−entangled ^{1}[T…T] state, which is driven by entropy because there could be many more possible configurations for ^{1}[T…T] than for ^{1}[TT].[8-10] ^{1}[T…T] then eventually decoheres into two free triplet excitons T_1 (Fig.1).[8-9] ^{1}[TT] and ^{1}[T…T] should be two different electronic states because the orbital overlap and interaction between the two triplet excitons is significantly reduced in ^{1}[T…T].[8, 11] The nature of the intermediate state ^{1}[TT] is currently under debate and has attracted significant research interests.[4-5, 7, 9, 11-28] Recently, the understanding of ^{1}[TT] has been addressed by using advanced ultrafast spectroscopic techniques and by employing covalently linked dimers in solution where the ^{1}[TT] state does not dissociate.[19, 22, 27, 29-32] Specifically, the electronic- and vibronic-coupling between ^{1}[TT] and S_1 states has been proposed to explain the rapid initial step in exciton fission.[5, 7, 18, 24, 33]

Despite the critical insights into the structure and dynamics of ^{1}[TT] provided by recent ultrafast spectroscopic measurements, there remain many open questions. For instance, the transport mechanism of ^{1}[TT] is largely unknown. ^{1}[TT] could be long-lived and potentially useful for multi-electron transfer reactions.[27-28, 34] Recent experiments

suggest that multi-electron transfer can occur from ^{1}[TT] with >100% photon-to-charge conversion efficiency.[25] Migration of ^{1}[TT] to sites with significant disorder (i.e., crystal defects or surfaces) has been proposed as the mechanism for the dissociation of triplet pairs in endothermic singlet fission.[28] Long-range transport of the entangled triplet pairs could also be promising for quantum information and spintronics applications.[15, 20] Further, understanding the ^{1}[TT] transport mechanism could shed light on the nature of the interaction between the ^{1}[TT] and S_1 states.

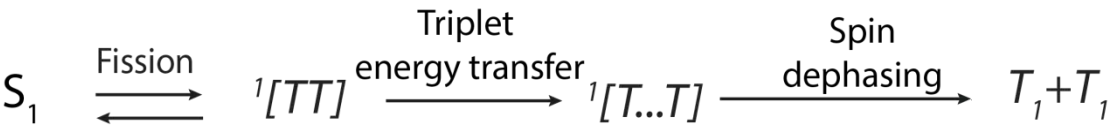

Figure 1. Schematic diagram of the singlet fission process.

Here we image temperature-dependent exciton transport in single crystals of tetracene employing transient absorption microscopy (TAM) to elucidate triplet pair migration. We have recently demonstrated TAM as a new means to image exciton transport in organic materials with ~ 200 fs temporal resolution and ~ 50 nm spatial precision.[35-37] These previous measurements have unraveled a new exciton transport picture for endothermic singlet fission materials, in which triplets can migrate as singlet excitons on nanosecond timescales much longer than the primary singlet fission time constant.[35] However, the transport of the intermediates was not considered in our original kinetic model. The challenges in imaging population transport within ^{1}[TT] include the spectral overlap of the ^{1}[TT], ^{1}[T…T], S_1, and T_1 states and the complex nature of singlet fission kinetics. To circumvent these difficulties, we image exciton diffusion in single tetracene crystals at temperatures as low as 5 K to differentiate the contribution from

^{1}[TT] by preventing its thermally-assisted evolution to isolated T_1 species.[10] Exciton transport modeling suggests that ^{1}[TT] is very mobile with a diffusion constant of 36 cm^2s^{-1} at 5 K, implying a transport mechanism similar to that of singlet excitons.

Temperature dependent triplet dynamics. We first perform temperature- and polarization- dependent transient absorption spectroscopy on a single tetracene crystal to elucidate state-specific dynamics. The crystal is positioned with the *a*-*b* plane parallel to the substrate. The pump at 470 nm is polarized parallel to the *b* axis and the probe polarization is set to either parallel or perpendicular to the *b* crystal axis (Fig. 2a). While the 470 nm excitation leads to the formation of vibrationally hot S_1 excitons, a previous report[38] demonstrated that singlet fission dynamics was independent of pump wavelength in tetracene, likely due to that vibrational relaxation occurs on a faster timescale than singlet fission. The bleach of the low energy Davydov band of the S_1 state centered at 520 nm is observed when probed parallel to the *b* axis, along with a much stronger stimulated emission peak at 536 nm. The magnitude of the photoinduced bleach and stimulated emission signal at 5K is about five-fold higher than at room temperature (RT) when excited with the same pump fluence (Fig. 2b), due to the superradiance effect resulting from singlet exciton delocalization at low temperatures.[39] Singlet exciton size has been estimated to be around 10 molecules at 4 K.[39] The bleaching of the high-energy Davydov component of the S_1 at 507 nm is predominately aligned perpendicular to the *b* axis[40] (Figs. 2c and 2d).

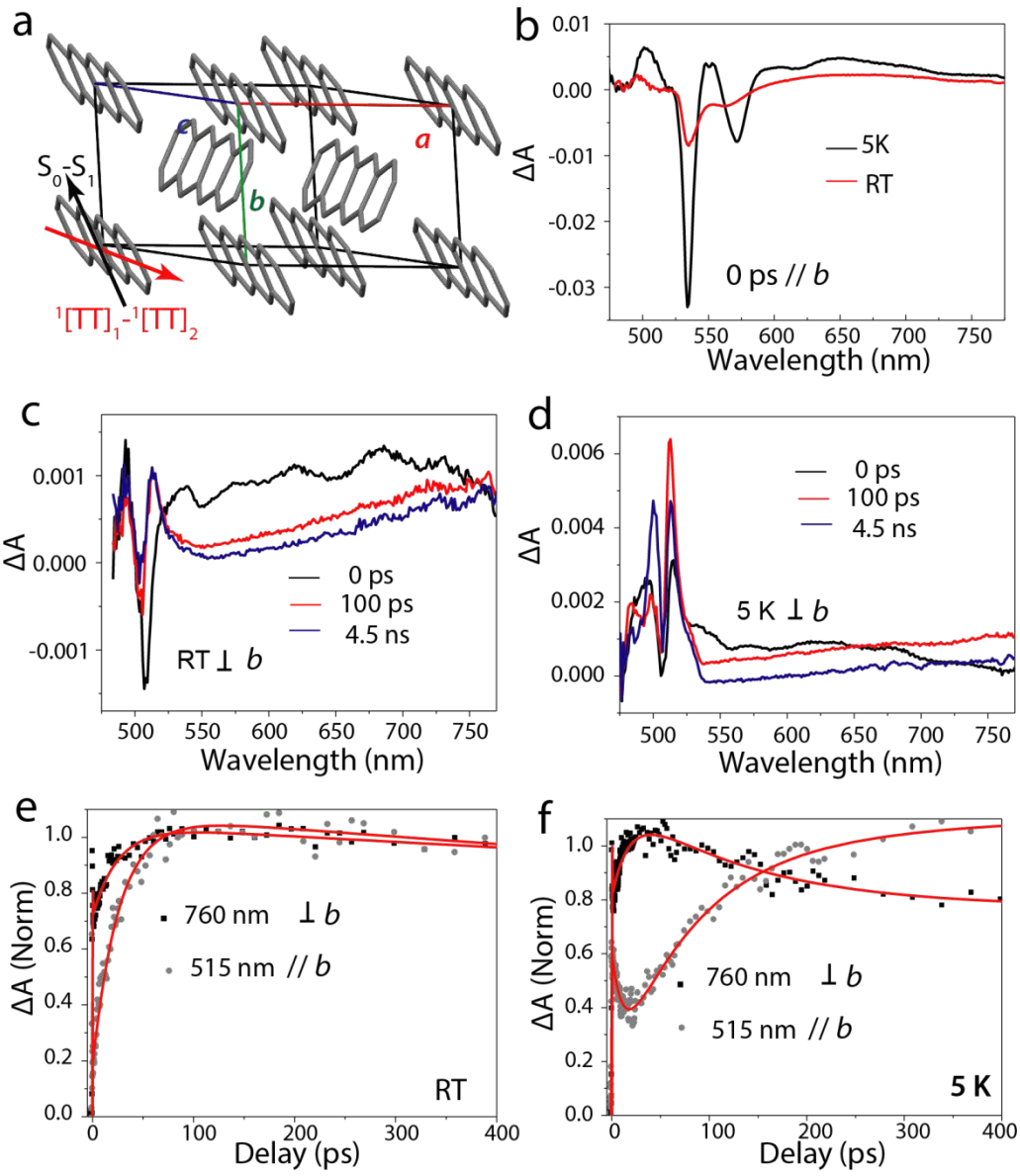

Figure 2. Temperature- and polarization- dependent transient absorption spectra and dynamics. (a) Crystal structure of tetracene plotted with singlet and triplet exciton transition dipole moments. (b) Transient absorption spectra at 0 ps delay probing parallel to the b axis at room temperature and at 5 K. Transient absorption spectra at different delays probing perpendicular to the b axis at room temperature (c) and at 5 K (d). Transient absorption dynamic traces probed at the excited state absorption (ESA) band near 760 nm and the ESA band near 515 nm at room temperature (e) and at 5 K (f). Pump = 470 nm, initial exciton density ≅ 1.8×10^{18} cm^{-3}. ΔA: change of absorbance.

There are new excited-state transitions in the near-infrared (NIR) region associated with ^{1}[TT] that are different from those from T_1 because of the strong interaction between the two triplet excitons in ^{1}[TT] with a binding energy as large as 100 meV.[22, 25, 27] Recent theoretical calculations have predicted that an excited-state absorption (ESA) band around

800 nm for pentacene is dominated by $^1[TT]_1$ to $^1[TT]_2$ transition, which is dipole–allowed and with larger oscillator strength than the T_1-T_2 transition.[41] The T_1-T_2 transition is forbidden in monomer tetracene solution and only becomes somewhat allowed in the crystals. Experimentally, pump−depletion−probe experiments on TIPS-pentacene have confirmed that the ESA band near 800 nm contains contribution from $^1[TT]$ in addition to T_1.[42] New $^1[TT]_1$ to $^1[TT]_2$ transition in the NIR spectral region has also been observed in pentacene dimers.[22]

In the visible spectral range, multiple long-lived ESA bands are observed between 480 nm and 550 nm when probing both parallel and perpendicular to the *b* axis due to the overlap between ESA and ground state bleaching bands (Figs. 2c and 2d, and Fig. S1), which are attributable to T_1 to T_n transitions.[24, 41, 43-45] S_1 to S_n ESA bands are also present in the visible spectral range, however, they decay much faster, on the order of 10s of picoseconds. We assume the spatially separated triplet pair $^1[T\ldots T]$ shares the spectrum of the isolated T_1 state because the correlation electronic energy is only ~ 60 neV for $^1[T\ldots T]$[46], much smaller than the binding energy for the two triplets in $^1[TT]$. [22, 25, 27]

The temperature dependence of the ESA bands at NIR and the visible spectral ranges reflects the dissociation of $^1[TT]$ to $^1[T\ldots T]$. The rise of the ESA at 515 nm corresponding to the formation of T_1 becomes slower as temperature decreases (Fig. 2 and Fig. S2), from 25 ± 4 ps at RT to a biexponential rise of 80 ± 20 ps and 3.5 ± 1.0 ns at 5 K. These observations are consistent with the dissociation of $^1[TT]$ to $^1[T\ldots T]$ being thermally activated.[10] At 5K, the risetime probed at 515 nm is much slower than when probed at 760 nm (Fig. 2f). This could be understood because $^1[TT]$ population at 5 K is

significant due to the slow dissociation, and it contributes more significantly to the NIR ESA band than to the visible ESA band. We attribute the risetime of 18 ± 5 ps probed at 760 nm to the buildup of the ^{1}[TT] population and the risetime of 80 ± 20 ps probed at 515 nm to the dissociation of ^{1}[TT] at 5 K. The ESA at 760 nm has a fast decay time of ~ 80 ps, also consistent with the dissociation of ^{1}[TT].

At RT, ^{1}[TT] dissociation to form ^{1}[T…T] becomes more rapid, on the order of a few picoseconds,[10] much faster than the generation of ^{1}[TT] from S_1 (~ 26 ps), leading to very low ^{1}[TT] population at steady state. Therefore, $S_1 \rightarrow$ ^{1}[TT] is the rate limiting step in forming ^{1}[T…T] and isolated T_1, and dynamics probing at 515 nm and 760 nm show nearly identical rise time of 25 ± 4 ps and 26 ± 1 ps, respectively (Fig. 2e). ^{1}[T…T] and isolated T_1 also contribute to the absorption in the NIR. Because the ^{1}[TT] population is low, probing at NIR or visible ESA bands should result in similar dynamics at RT, which is observed experimentally as shown in Figure 2e. We ascribed the NIR absorption at RT to T_1 and ^{1}[T…T] in our previous publication,[35] which does not contradict our assignment here because of the negligible steady-state ^{1}[TT] population.

The bi-exponential rise of the T_1 ESA signal at 5 K indicates that there exist at least two pathways for the formation of T_1. In contrast, the second and slower pathway is not observed at RT. To unravel these two pathways, we perform target analysis of the entire set of spectra at 5 K,[47-48] using a kinetic model with two parallel pathways (schematically shown in Fig. 3a). We obtain the singlet lifetime of 10 ± 1 ps by fitting to the decay of singlet ESA band at 610 nm (Fig. S4). The ^{1}[TT] formation time of 18 ps, and the ^{1}[T…T] formation times of 80 ps, and 3.5 ns are determined from the dynamics results

shown in Fig. 2 and Fig. S3. The resulting species-associated spectra (SAS) at 5 K from the targeted global analysis are presented in Fig. 3 and Fig. S5. The spectrum of ^{1}[TT] shows overall similar vibrational progressions as the S_1 state, consistent with a previous report.[22] The intermediate state leading to formation of T_1 with a 3.5 ns time constant shows distinct spectral features from both the S_1 and T_1 states (Fig. 3c and Fig. S5). Specifically, we determine the formation time of this slow intermediate state to be 27 ± 3 ps (Fig. S6) using the ESA band at 481 nm that is distinct from the other states (Fig. 3c).

A possible origin for the slow intermediate state at 5 K is that the singlet excitons can be 'trapped' at crystal defects or low energy sites at low temperatures, where exciton diffusion by resonant-energy transfer is slowed or stopped. At RT, the trapped and free singlet exciton population distribution strongly favors free excitons and therefore such trap states are not observed. Time dependent PL spectra also support the existence of such trap state (Fig. S7). At 5 K, redshifted emission at ~ 630 nm grows in at longer delay times and displays much slower PL decay with a few ns lifetime (Fig. S7), indicating trap state emission, consistent with a previous report.[39] It is possible that the emission 630 nm contains contribution from ^{1}[TT]. However, the dissociation of ^{1}[TT] to ^{1}[T…T] occurs at ~ 80 ps, which means the vast majority of ^{1}[TT] state should dissociate, instead of emitting. At RT, PL decays uniformly across all wavelengths, consistent with S_1 being the only emitting state (Fig. S7).

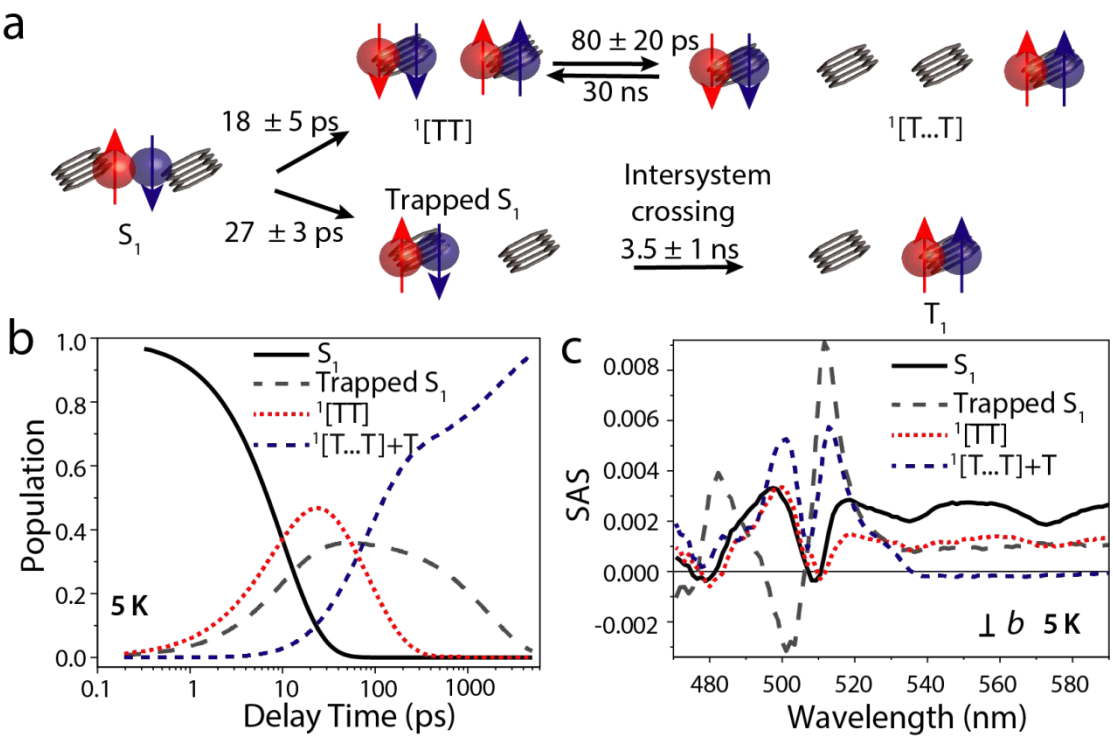

Figure 3. Singlet fission mechanism pathway at 5 K**.** (a) Schematic illustration of the kinetic model for singlet fission at 5K. (b) Population dynamics of the different species from the target analysis. (c) Species-associated spectra (SAS) perpendicular to the b axis of all the excited states involved in the singlet fission process obtained by target analysis of the transient absorption spectra at 5 K.

Possible crystal defects are stacking faults that occur parallel to the basic slip plane of the crystal, e.g., the *a*-*b* plane[49]. Such stacking faults lead to two molecules situated in parallel positions forming a so called predimer state,[49] which could serve as an energetic trap. A phase transition in crystalline tetracene occurring at around 150 K could also contribute to the formation of the trapped singlet excitons[50-52]. Defect trapped singlet excitons have been proposed based on low temperature dynamics measurements in tetracene thin films.[45] Once trapped, the singlet exciton is less likely to undergo fission because of the reduced coupling to the ^{1}[TT] state.[53] Instead, triplet formation can occur via intersystem crossing in competition with trapped exciton emission. The slow formation time (3.5 ns) of the second pathway for T_1 is in good agreement with the intersystem crossing time of 4 ns determined for monomer tetracene in solution.[45]

Because trapping of S_1 and generation of ^{1}[TT] are competing processes, ^{1}[TT] is more likely to be generated at locations away from the crystal faults. Therefore, trapping of ^{1}[TT] is less likely or at least slower and therefore probably not competitive with ^{1}[TT] decay to [T…T]. We do not consider the trapping of ^{1}[TT] here, which could lead to underestimation of the diffusion constant of ^{1}[TT].

Temperature-dependent singlet and triplet exciton transport. Because ^{1}[TT] is much longer-lived at low temperatures and with a larger steady-state population,[10] we image exciton transport using TAM at three different temperatures (RT, 150 K and 5 K) to elucidate how triplet excitons transport while bound within the ^{1}[TT] state. The crystal is positioned with the *a*-*b* plane parallel to the substrate and the pump wavelength is at 470 nm, creating S_1 excitons initially. Because of the reduced heat capacity of tetracene, photoinduced heating of the sample could be significant at 5 K. The absorbance difference due to the thermal effects is plotted in Fig. S9, showing that thermal effects are most significant for wavelengths shorter than 550 nm. Therefore, we choose probe wavelengths of 700 nm and 800 nm that are far away from ground state absorption to minimize thermal effects as well as the interference from PL. Figs. 4a and 4c illustrate TAM images with probe wavelength and polarization perpendicular to the *b* axis selected to preferentially image the ESA band that contains more significant contribution from ^{1}[TT] at 810 nm. As indicated by the long-lived dynamics in the ns timescales (Fig. S8), ^{1}[T…T] and possible T_1 also contribute at this wavelength. In principle, the motion of ^{1}[T…T] and isolated T_1 can be imaged at ~ 515 nm, however, thermal effects and large overlap with singlet transitions make such experiments very challenging. The S_1 and

trapped S_1 are imaged at the ESA band at 700 nm with probe polarization parallel to the *b* axis.

To image exciton transport, the pump beam is held at a fixed position while the probe beam is scanned relative to the pump with a Galvanometer scanner and the pump induced change in probe transmission (ΔT) is plotted as a function of probe position to form an image (Fig. S10), more details in Methods section in the Supporting Information (SI).[35] The two-dimensional (2D) TAM images are shown in Fig. 4 and Fig. S11. The exciton transport processes is considered as diffusion in the *a*–*b* plane because the crystal is positioned with the *a*-*b* plane parallel to the substrate and ΔT is integrated over the *c* axis[35]. The initial population n ($x, y, 0$) follows a 2D Gaussian distribution as created by a Gaussian pump beam at position (x_0, y_0) with a pulse duration of ~ 300 fs:

$$n(x,y,0) = Nexp[-\frac{(x-x_0)^2}{2\sigma(0)_x^2} - \frac{(y-y_0)^2}{2\sigma(0)_y^2}] \quad (1)$$

As shown in Figs. 4b and 4d, the population distribution at any later time *t* also follows a Gaussian function,

$$n(x,y,t) = Nexp[-\frac{(x-x_0)^2}{2\sigma(t)_x^2} - \frac{(y-y_0)^2}{2\sigma(t)_y^2}] \quad (2)$$

We obtain exciton transport distance along the *b* axis L by $L^2 = \sigma(t)_b^2 - \sigma(0)_b^2$.[35, 54] Figs. 5a and 5b show the temperature dependent time evolution of L^2 for probing at 810 nm and 700 nm, respectively.

Singlet exciton migration accelerates as temperature decreases (Fig. 5a), consistent with previous transient grating measurements of singlet transport in anthracene crystals.[55] Such temperature dependence suggests that exciton delocalization plays a role. Delocalized excitons can accelerate transport as compared to Förster hopping involving

localized excitations, because the delocalization size defines an effective hopping length that can be much larger than the nearest-neighbor intermolecular spacings.[37, 56] Excitons become more delocalized at lower temperature due to reduced exciton-phonon scattering rate, agreeing with the superradiance effect shown in Fig. 2b. At low temperatures, singlet transport slows down after 20 ps, due to the trapping of singlet excitons by defects sites occurring at this timescale.

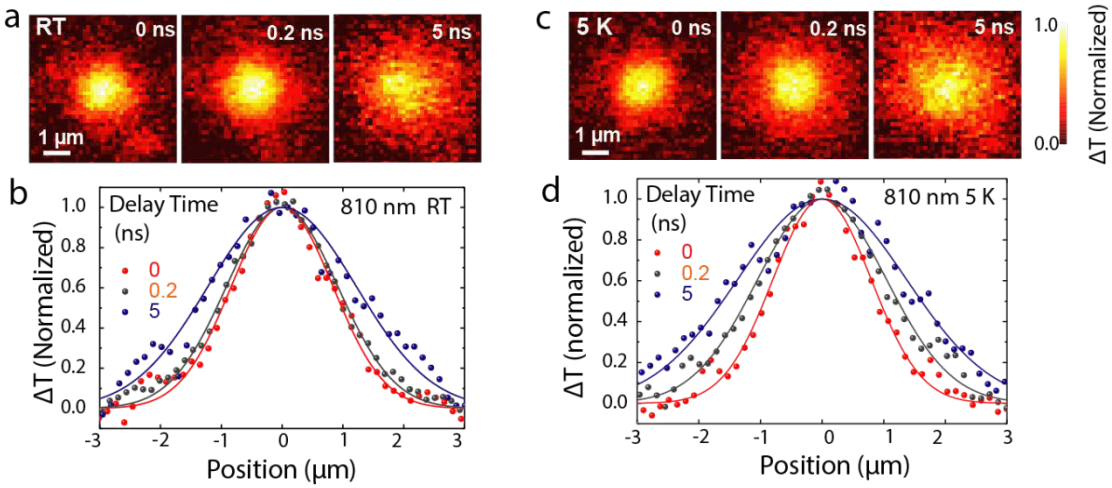

Figure 4. Temperature dependent triplet propagation imaged with probe wavelength of 810 nm. TAM images in the *a*-*b* plane pumped at 470 nm (initial excitation density 5.0 $\times 10^{19}$ cm^{-3}) and probed at 810 nm with polarization to select triplet excitons at different delay pump-probe delays at room temperature (a) and 5 K (c). Color scale represents the intensity of pump-induced differential transmission (ΔT) of the probe and every image has been normalized by peak value. (c) and (d) Cross-sections of the TAM images fitted with Gaussian functions along the *b* axis, with the maximum ΔT signal normalized.

As shown in Fig. 4 and Fig. 5b, exciton motion imaged at 810 nm also migrates at a faster rate as temperature decreases. For instance, L^2 is about twice larger at 5 K than at RT at 200 ps delay. This temperature dependence cannot be explained by intrinsic T_1 transport as it is predicted to be largely temperature independent.[57] Because ^{1}[TT] is much longer-lived and with larger population at low temperatures, it is most likely that ^{1}[TT] plays a more significant role for transport at lower temperatures.

Interestingly, exciton motion imaged at 810 nm is more rapid than that at 700 nm for

temperatures below 150 K and for delay times between 10 ps and 100 ps (Fig. 5c and Fig. S12). At RT, we have discovered a new singlet-mediated pathway that allows for triplet excitons to migrate as singlet excitons long after the singlet fission time scale in tetracene.[35-36] However, the singlet-mediated mechanism cannot explain the observations of Fig. 5c and Fig. S12. A singlet-mediated mechanism should lead to similar transport on the 100 ps timescale due to the interconversion of population between the two states, which is observed when imaged at RT as shown in Fig. 5d. The rapid transport imaged at 810 nm suggests that ^{1}[TT] is mobile at low temperatures. Also, the more rapid motion imaged at 810 nm than that imaged at 700 nm after 10 ps (Fig. 5c) indicates that the regeneration of S_1 from ^{1}[TT] is inefficient at 5K, which could be explained by that ^{1}[TT] might be slightly lower in energy than S_1 for tetracene when including the ^{1}[TT] state binding energy as large as 100 meV.[22, 25, 27] The energetics are also consistent with the lack of temperature dependence in the formation of ^{1}[TT] (Fig. S2). Thus, the quantum beats observed in the PL dynamics for tetracene at low temperatures reported previously[13, 15] could be due to the interconversion between ^{1}[TT] and ^{1}[T…T] states, instead of the interconversion between ^{1}[TT] and S_1.

Transport of the ^{1}[TT] state. To extract key parameters for the transport of ^{1}[TT], we model the data in Fig. 5 with coupled rate equations that describe the population as function of space and time for free S_1, trapped S_1, ^{1}[TT], ^{1}[T…T], and T_1, which are detailed in the SI, equations S1-S8. We adopt previously reported values for the radiative rate of singlet and triplet excitons, k_S and k_T to be 12.5 ns[58] 62.5 μs[59], respectively. The regeneration rate of ^{1}[TT] from the ^{1}[T…T] state $k_{T...T\text{-}TT}$ and the dissociation rate of

^{1}[T…T] to form isolated T_1 $k_{dissociation}$ obtained from fitting the TAM transport data. We use a time constant of 20 ns as a starting point for $k_{dissociation}$ based on the dephasing of ^{1}[T…T] measured by quantum beat damping in PL dynamics.[13] Other rate constants are extracted from the transient absorption measurements and target analysis as detailed in Table S1. The initial singlet exciton density we used is 5.0×10^{19} cm^{-3}, which is above the annihilation threshold as reported in Ref.[54]. To correctly simulate the transport data, exciton-exciton annihilation processes need to be considered, as described in the SI, equations S9-S14. In addition to the annihilation processed in our original model,[35] we also include here annihilation of T_1 to T_n for completeness. In the original model, this loss of T_1 population was accounted in the annihilation between T_1 and S_1. The annihilation rates are obtained by global fitting of the density dependent exciton dynamics (Fig. 5 and Fig. S13). Note that the annihilation rates are lower than what we reported in our previous work.[35] In this study, we have studied a wider range of exciton density to more accurately determine annihilation rates.

With these considerations, the coupled rate equations S15-S19 presented in the SI describe the transport and dynamics of the different exciton populations. n_{S1}, n_{TT}, $n_{trapped}$, $n_{T...T}$, and n_T are the density of S_1, ^{1}[TT], trapped S_1, ^{1}[T…T], and T_1, respectively. D_s is the diffusion coefficient of singlet exciton, D_{TT} is that of ^{1}[TT] state, and D_T is that of the triplet exciton. We set the diffusion constant of trapped $S_1$to 0. The values of D_T and $D_{T...T}$ are set to be the same, and we adopt the value of 0.0023 cm^{2}s^{-1} reported by Akselrod et al.[54]. We do not vary D_T and $D_{T...T}$ as a function of temperature, as theoretical calculation suggested triplet diffusion to be weakly temperature dependent.[57] D_s and D_{TT} are adjusted

to best fit the temperature dependent transport data. Fixed and free parameters are indicated in Table S1. Spectral overlap between the singlet, trapped singlet, ^{1}[TT], ^{1}[T…T], and free triplet excited state needs to be taken into account to correctly model the data, and the weight of different species extracted from the fitting are given in Table S2.

As shown in Fig. 5 and Figs. S12, S13 and S14, the same set of parameters reproduce the whole experimental data set satisfactorily well, including both the spatial profiles and the dynamics. The most critical fitting parameters are D_s and D_{TT}. To demonstrate the sensitivity to the fitting parameters, the fitting results when varying D_s and D_{TT} by ± 20 % are shown in Fig. S15. In our original model[35], we did not differentiate between ^{1}[TT] and ^{1}[T…T]. These two models can be reconciled when considering that the dissociation of ^{1}[TT] to form ^{1}[T…T] (1ps) is much more rapid than the generation of ^{1}[TT] from S_1 (27ps) leading to very low steady-state ^{1}[TT] population at RT.

Singlet excitons are very mobile at 5 K, with a diffusion constant of 52 cm^2s^{-1}, an order of magnitude higher than that of 3.8 cm^2s^{-1} at RT. At low temperatures, the motion of singlet excitons slows down after 20 ps because the singlet population either has converted to ^{1}[TT] or being trapped and the trapped singlet excitons have very low mobility. The kinetic modeling suggests that the mobile ^{1}[TT] is likely to be responsible for the accelerated exciton transport imaged at 810 nm at low temperatures. The diffusion constant of ^{1}[TT] increases from 22 cm^2s^{-1} at 150 K to 36 cm^2s^{-1} at 5 K. It is not possible to extract a meaningful D_{TT} at RT due to its short lifetime and low population. The equilibrium between ^{1}[T…T] and ^{1}[TT] dominates the overall triplet transport at low

temperatures. Because the diffusion constant for ^{1}[TT] is orders of magnitude higher than the D_T and $D_{T\ldots T}$, the intrinsic diffusion of ^{1}[T…T] and T_1 play a negligible role (changing the values of D_T and $D_{T\ldots T}$ by more than one order of magnitude does not change the fitting results).

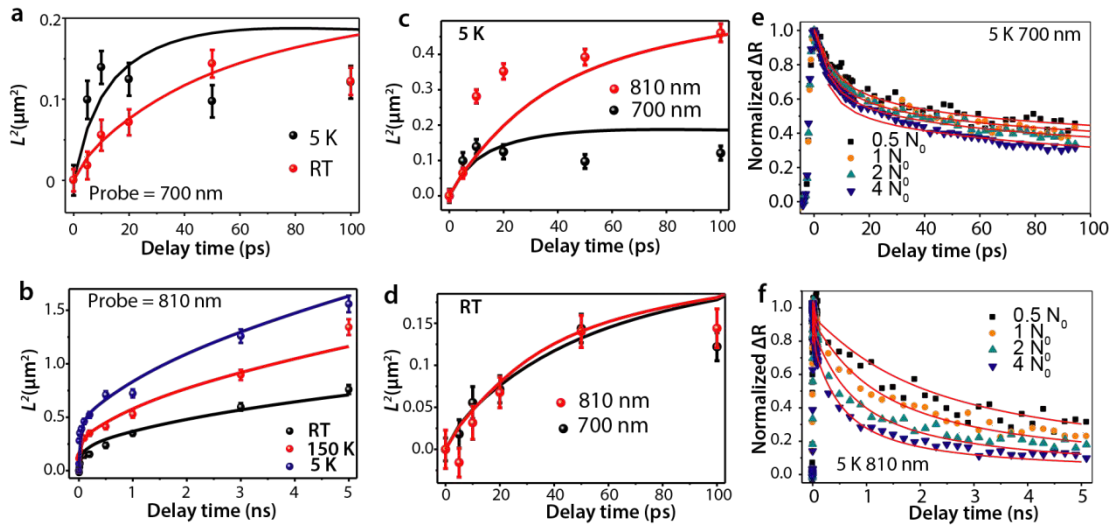

Figure 5. Kinetic modeling of temperature-dependent exciton migration. Temperature dependent time evolution of $L^2 = \sigma(t)_b^2 - \sigma(0)_b^2$ for probing at 700 nm (a) and 810 nm (b), respectively. Error bars are the standard error estimated from the 2D Gaussian fitting to the spatial intensity distribution. (c) and (d) Comparison of the time evolution of L^2 for probing at 700 nm and 810 nm at 5 K and at room temperature, respectively. Simulated time evolution of L^2 are shown in solid lines. (e) and (f) Experimental and simulated exciton density dependent kinetics, probed at the central of pump location for probing at 700 nm and 810 nm, respectively. The initial exciton densities are given as multiples of $N_0 = 5.0 \times 10^{19}$ cm^{-3}.

A diffusion constant as high as 36 cm^{2}s^{-1} indicates that the transport mechanism of ^{1}[TT] state must be similar to that of singlet excitons because the triplet excitons have much lower diffusion constants. ^{1}[TT] is likely not a strictly dark state, as the transition dipole moment of S_0-^{1}[TT] transition has been calculated to be approximately one third of that of the bright S_0-S_1 transition.[23] The accelerated transport at low temperatures (Fig. 5b) suggests that ^{1}[TT] taking on the delocalized nature of singlet exciton, probably resulting from the electronic coupling between ^{1}[TT] with S_1.[24] The delocalization of the ^{1}[TT] state implies that singlet fission involves molecules that are not nearest to each

other at low temperature.[15] Another possibility is through Herzberg−Teller mechanism in which ^{1}[TT] couples vibronically to the S_1 state.[60] The vibronic coupling effectively breaks the symmetry of the ^{1}[TT] state, enabling intensity borrowing from the allowed S_0 to S_1 transition.[60] The phase transition occurring at around 150 K leads to small and subtle changes in the crystal structures, which could also affect the intermolecular couplings.[52] A thorough understanding of the transport mechanism for ^{1}[TT] requires further experimental and theoretical investigations.

In addition to the implications in singlet fission, these mobile triplet-pair states could open new avenues for applications in quantum information and spintronics.[15, 20] Recent theoretical calculations and experimental results show that spin coherence can be maintained by the two spatially separated triplet excitons in the ^{1}[T…T] state[8], and experiments have verified that ^{1}[T…T] state can live for milliseconds in tetracene.[20] Transport within ^{1}[TT] and ^{1}[T…T] states extracted from our model at 5 K is shown in Fig. S16. Long-range triplet pair transport resulting from the interconversion of the ^{1}[TT] and ^{1}[T…T] states at low temperatures observed here could provide a solution for controlling entanglement over long distance.

In conclusion, we have imaged the transport of ^{1}[TT] state in single tetracene crystals employing temperature-dependent TAM. Our data analysis suggests that ^{1}[TT] is very mobile, with a diffusion constant of 36 cm^2s^{-1} at 5 K, similar to that of free singlet excitons. The motion of ^{1}[TT] accelerates at low temperatures, likely due to exciton delocalization. These results suggest that ^{1}[TT] shares a similar transport mechanism with

bright singlet exciton, which could have important implications in designing materials for singlet fission and spintronics applications.

ASSOCIATED CONTENT: Supporting Information describes, nethods, kinetic modeling, and supporting figures and tables. Supporting Information is available free of charge *via* the internet at http://pubs.acs.org.

Acknowledgements

L.H. and Y.W. acknowledge support from US National Science Foundation through grant NSF-CHE-1555005. J.C.J. acknowledges the Solar Photochemistry Program supported by the U.S. Department of Energy, Office of Basic Energy Sciences, Division of Chemical Sciences, Biosciences, and Geosciences under Contract No. DE-AC36-08GO28308 with NREL. Use of the Center for Nanoscale Materials, an Office of Science user facility, was supported by the U.S. Department of Energy, Office of Science, Office of Basic Energy Sciences, under Contract No. DE-AC02-06CH11357. The views expressed in the article do not necessarily represent the views of the DOE or the U.S. Government. The U.S. Government retains and the publisher, by accepting the article for publication, acknowledges that the U.S. Government retains a nonexclusive, paid-up, irrevocable, worldwide license to publish or reproduce the published form of this work, or allow others to do so, for U.S. Government purposes.

Competing financial interests: The authors declare no competing financial interest.

References:

(1) Smith, M. B.; Michl, J., Recent advances in singlet fission. *Annu Rev Phys Chem* **2013**, *64*, 361-386.

(2) Congreve, D. N.; Lee, J.; Thompson, N. J.; Hontz, E.; Yost, S. R.; Reusswig, P. D.;

Bahlke, M. E.; Reineke, S.; Van Voorhis, T.; Baldo, M. A., External quantum efficiency above 100% in a singlet-exciton-fission-based organic photovoltaic cell. *Science* **2013**, *340*, 334-337.

(3) Zimmerman, P. M.; Zhang, Z.; Musgrave, C. B., Singlet fission in pentacene through multi-exciton quantum states. *Nat Chem* **2010**, *2*, 648-652.

(4) Chan, W.-L.; Ligges, M.; Jailaubekov, A.; Kaake, L.; Miaja-Avila, L.; Zhu, X.-Y., Observing the multiexciton state in singlet fission and ensuing ultrafast multielectron transfer. *Science* **2011**, *334*, 1541-1545.

(5) Chan, W.-L.; Ligges, M.; Zhu, X.-Y., The energy barrier in singlet fission can be overcome through coherent coupling and entropic gain. *Nat Chem* **2012**, *4*, 840-845.

(6) Aryanpour, K.; Shukla, A.; Mazumdar, S., Theory of singlet fission in polyenes, acene crystals, and covalently linked acene dimers. *J Phys Chem C* **2015**, *119*, 6966-6979.

(7) Stern, H. L.; Cheminal, A.; Yost, S. R.; Broch, K.; Bayliss, S. L.; Chen, K.; Tabachnyk, M.; Thorley, K.; Greenham, N.; Hodgkiss, J. M.; Anthony, J.; Head-Gordon, M.; Musser, A. J.; Rao, A.; Friend, R. H., Vibronically coherent ultrafast triplet-pair formation and subsequent thermally activated dissociation control efficient endothermic singlet fission. *Nat Chem* **2017**, *9*, 1205-1212.

(8) Scholes, G. D., Correlated pair states formed by singlet fission and exciton–exciton annihilation. *J. Phys. Chem. A* **2015**, *119*, 12699-12705.

(9) Breen, I.; Tempelaar, R.; Bizimana, L. A.; Kloss, B.; Reichman, D. R.; Turner, D. B., Triplet separation drives singlet fission after femtosecond correlated triplet pair production in rubrene. *J Am Chem Soc* **2017**, *139*, 11745-11751.

(10) Lee, T. S.; Lin, Y. L.; Kim, H.; Pensack, R. D.; Rand, B. P.; Scholes, G. D., Triplet energy transfer governs the dissociation of the correlated triplet pair in exothermic singlet fission. *J. Phys. Chem. Lett.* **2018**, *9*, 4087-4095.

(11) Grieco, C.; Kennehan, E. R.; Kim, H.; Pensack, R. D.; Brigeman, A. N.; Rimshaw, A.; Payne, M. M.; Anthony, J. E.; Giebink, N. C.; Scholes, G. D.; Asbury, J. B., Direct observation of correlated triplet pair dynamics during singlet fission using ultrafast mid-ir spectroscopy. *J. Phys. Chem. C* **2018**, acs.jpcc.7b11228.

(12) Greyson, E. C.; Vura-Weis, J.; Michl, J.; Ratner, M. A., Maximizing singlet fission in organic dimers: theoretical investigation of triplet yield in the regime of localized excitation and fast coherent electron transfer. *J Phys Chem B* **2010**, *114*, 14168-14177.

(13) Burdett, J. J.; Bardeen, C. J., Quantum beats in crystalline tetracene delayed fluorescence due to triplet pair coherences produced by direct singlet fission. *J Am Chem Soc* **2012**, *134*, 8597-8607.

(14) Beljonne, D.; Yamagata, H.; Brédas, J.; Spano, F.; Olivier, Y., Charge-transfer excitations steer the Davydov splitting and mediate singlet exciton fission in pentacene. *Phys Rev Lett* **2013**, *110*, 226402.

(15) Wang, R.; Zhang, C.; Zhang, B.; Liu, Y.; Wang, X.; Xiao, M., Magnetic dipolar interaction between correlated triplets created by singlet fission in tetracene crystals. *Nat Comm* **2015**, *6*, 8602.

(16) Stern, H. L.; Musser, A. J.; Gelinas, S.; Parkinson, P.; Herz, L. M.; Bruzek, M. J.; Anthony, J.; Friend, R. H.; Walker, B. J., Identification of a triplet pair intermediate in singlet exciton fission in solution. *PNAS* **2015**, *112*, 7656-7661.

(17) Bakulin, A. A.; Morgan, S. E.; Kehoe, T. B.; Wilson, M. W.; Chin, A. W.; Zigmantas, D.; Egorova, D.; Rao, A., Real-time observation of multiexcitonic states in ultrafast singlet fission using coherent 2D electronic spectroscopy. *Nat Chem* **2016**, *8*, 16-23.
(18) Monahan, N. R.; Sun, D.; Tamura, H.; Williams, K. W.; Xu, B.; Zhong, Y.; Kumar, B.; Nuckolls, C.; Harutyunyan, A. R.; Chen, G.; Dai, H. L.; Beljonne, D.; Rao, Y.; Zhu, X. Y., Dynamics of the triplet-pair state reveals the likely coexistence of coherent and incoherent singlet fission in crystalline hexacene. *Nat Chem* **2017**, *9*, 341-346.
(19) Tayebjee, M.; Sanders, S. N.; Kumarasamy, E., Quintet multiexciton dynamics in singlet fission. *Nat Phys* **2017**, *13*, 182-188.
(20) Weiss, L. R.; Bayliss, S. L.; Kraffert, F.; Thorley, K. J.; Anthony, J. E.; Bittl, R.; Friend, R. H.; Rao, A.; Greenham, N. C.; Behrends, J., Strongly exchange-coupled triplet pairs in an organic semiconductor. *Nat Phys* **2016**, *13*, 176-181.
(21) Pensack, R. D.; Ostroumov, E. E.; Tilley, A. J.; Mazza, S.; Grieco, C.; Thorley, K. J.; Asbury, J. B.; Seferos, D. S.; Anthony, J. E.; Scholes, G. D., Observation of two triplet-pair intermediates in singlet exciton fission. *J Phys Chem Lett* **2016**, *7*, 2370-2375.
(22) Trinh, M. T.; Pinkard, A.; Pun, A. B.; Sanders, S. N.; Kumarasamy, E.; Sfeir, M. Y.; Campos, L. M.; Roy, X.; Zhu, X. Y., Distinct properties of the triplet pair state from singlet fission. *Sci Adv* **2017**, *3*, e1700241.
(23) Tempelaar, R.; Reichman, D. R., Vibronic exciton theory of singlet fission. I. Linear absorption and the anatomy of the correlated triplet pair state. *J. Chem. Phys.* **2017**, *146*, 174703.
(24) Chien, A. D.; Zimmerman, P. M., Recovering dynamic correlation in spin flip configuration interaction through a difference dedicated approach. *J. Chem. Phys.* **2017**, *146*, 014103.
(25) Yong, C. K.; Musser, A. J.; Bayliss, S. L.; Lukman, S.; Tamura, H.; Bubnova, O.; Hallani, R. K.; Meneau, A.; Resel, R.; Maruyama, M.; Hotta, S.; Herz, L. M.; Beljonne, D.; Anthony, J. E.; Clark, J.; Sirringhaus, H., The entangled triplet pair state in acene and heteroacene materials. *Nat Comm* **2017**, *8*, 15953.
(26) Bera, K.; Douglas, C. J.; Frontiera, R. R., Femtosecond raman microscopy reveals structural dynamics leading to triplet separation in rubrene singlet fission. *J. Phys. Chem. Lett.* **2017**, 5929-5934.
(27) Folie, B. D.; Haber, J. B.; Refaely-Abramson, S.; Neaton, J. B.; Ginsberg, N. S., Long-lived correlated triplet pairs in a pi-stacked crystalline pentacene derivative. *J Am Chem Soc* **2018**, *140*, 2326-2335.
(28) Thampi, A.; Stern, H. L.; Cheminal, A.; Tayebjee, M. J. Y.; Petty II, A. J.; Anthony, J. E.; Rao, A., Elucidation of excitation energy dependent correlated triplet pair formation pathways in an endothermic singlet fission system. *J. Am. Chem. Soc.* **2018**, *140*, 4613-4622.
(29) Zirzlmeier, J.; Lehnherr, D.; Coto, P. B.; Chernick, E. T.; Casillas, R.; Basel, B. S.; Thoss, M.; Tykwinski, R. R.; Guldi, D. M., Singlet fission in pentacene dimers. *PNAS* **2015**, *112*, 5325-5330.
(30) Sanders, S. N.; Kumarasamy, E.; Pun, A. B.; Trinh, M. T.; Choi, B.; Xia, J.; Taffet, E. J.; Low, J. Z.; Miller, J. R.; Roy, X.; Zhu, X. Y.; Steigerwald, M. L.; Sfeir, M. Y.; Campos, L. M.,
Quantitative intramolecular singlet fission in bipentacenes. *J. Amer. Chem. Soc.* **2015**, *137*,

8965-8972.
(31) Korovina, N. V.; Das, S.; Nett, Z.; Feng, X.; Joy, J.; Haiges, R.; Krylov, A. I.; Bradforth, S. E.; Thompson, M. E., Singlet fission in a covalently linked cofacial alkynyltetracene dimer. *J Am Chem Soc* **2016**, *138*, 617-627.
(32) Wu, Y.; Wang, Y.; Chen, J.; Zhang, G.; Yao, J.; Zhang, D.; Fu, H., Intramolecular singlet fission in an antiaromatic polycyclic hydrocarbon. *Angew. Chem. Int. Ed.* **2017**, *56*, 9400-9404.
(33) Grumstrup, E. M.; Johnson, J. C.; Damrauer, N. H., Enhanced triplet formation in polycrystalline tetracene films by femtosecond optical-pulse shaping. *Phys. Rev. Lett.* **2010**, *105*, 257403.
(34) Kim, H.; Keller, B.; Ho-Wu, R.; Abeyasinghe, N.; Vázquez, R. J.; Goodson III, T.; Zimmerman, P. M., Enacting two-electron transfer from a double-triplet state of intramolecular singlet fission. *J. Am. Chem. Soc.* **2018**, 140, 7760-7763.
(35) Wan, Y.; Guo, Z.; Zhu, T.; Yan, S.; Johnson, J.; Huang, L., Cooperative singlet and triplet exciton transport in tetracene crystals visualized by ultrafast microscopy. *Nat Chem* **2015**, *7*, 785-792.
(36) Zhu, T.; Wan, Y.; Guo, Z.; Johnson, J.; Huang, L., Two birds with one stone: tailoring singlet fission for both triplet yield and exciton diffusion length. *Adv Mater* **2016**, *28*, 7539-7547.
(37) Wan, Y.; Stradomska, A.; Knoester, J.; Huang, L., Direct imaging of exciton transport in tubular porphyrin aggregates by ultrafast microscopy. *J. Am. Chem. Soc.* **2017**, *139*, 7287-7293.
(38) Burdett, J. J.; Gosztola, D.; Bardeen, C. J., The dependence of singlet exciton relaxation on excitation density and temperature in polycrystalline tetracene thin films: Kinetic evidence for a dark intermediate state and implications for singlet fission. *J Chem Phys* **2011**, *135*, 214508.
(39) Lim, S.-H.; Bjorklund, T. G.; Spano, F. C.; Bardeen, C. J., Exciton delocalization and superradiance in tetracene thin films and nanoaggregates. *Phys Rev Lett* **2004**, *92*, 107402.
(40) Birech, Z.; Schwoerer, M.; Schmeiler, T.; Pflaum, J.; Schwoerer, H., Ultrafast dynamics of excitons in tetracene single crystals. *J Chem Phys* **2014**, *140*, 114501.
(41) Khan, S.; Mazumdar, S., Theory of transient excited state absorptions in pentacene and derivatives: triplet–triplet biexciton versus free triplets. *J. Phys. Chem. Lett.* **2017**, 5943-5948.
(42) Herz, J.; Buckup, T.; Paulus, F.; Engelhart, J. U.; Bunz, U. H. F.; Motzkus, M., Unveiling singlet fission mediating states in tips-pentacene and its aza derivatives. *J. Phys. Chem. A* **2015**, *119*, 6602-6610.
(43) Meyer, Y. H., Triplet-triplet spectroscopy of polyacenes. *J Chem Phys* **1972**, *56*, 801.
(44) Pati, Y. A.; Ramasesha, S., Exact solution of the ppp model for correlated electronic states of tetracene and substituted tetracene. *J. Phys. Chem. A* **2014**, *118*, 4048-4055.
(45) Burdett, J. J.; Müller, A. M.; Gosztola, D.; Bardeen, C. J., Excited state dynamics in solid and monomeric tetracene: The roles of superradiance and exciton fission. *J Chem Phys* **2010**, *133*, 144506.
(46) Bayliss, S. L.; Chepelianskii, A. D.; Sepe, A.; Walker, B. J.; Ehrler, B.; Bruzek, M. J.; Anthony, J. E.; Greenham, N. C., Geminate and nongeminate recombination of triplet excitons formed by singlet fission. *Phys Rev Lett* **2014**, *112*, 238701.

(47) Williams, R. M.; Vân Anh, N. n.; van Stokkum, I. H., Triplet formation by charge recombination in thin film blends of perylene red and pyrene: developing a target model for the photophysics of organic photovoltaic materials. *J Phys Chem B* **2013**, *117*, 11239-11248.
(48) Snellenburg, J. J.; Laptenok, S. P.; Seger, R.; Mullen, K. M.; van Stokkum, I. H., Glotaran: a Java-based graphical user interface for the R package TIMP. *J. Stat. Softw* **2012**, *49*, 1-22.
(49) Silinsh, E. A., *Organic Molecular Crystals*; Springer Berlin Heidelberg: Berlin, Heidelberg, 1980; Vol. 16.
(50) Venuti, E.; Della Valle, R. G.; Farina, L.; Brillante, A.; Masino, M.; Girlando, A., Phonons and structures of tetracene polymorphs at low temperature and high pressure. *Phys Rev B* **2004**, *70*, 104106.
(51) Sondermann, U.; Kutoglu, A.; Bässler, H., X-ray diffraction study of the phase transition in crystalline tetracene. *J Phys Chem* **1985**, *89*, 1735-1741.
(52) Arias, D. H.; Ryerson, J. L.; Cook, J. D.; Damrauer, N. H.; Johnson, J. C., Polymorphism influences singlet fission rates in tetracene thin films. *Chemical Science* **2016**, *7*, 1185-1191.
(53) Chan, W. L.; Berkelbach, T. C.; Provorse, M. R.; Monahan, N. R.; Tritsch, J. R.; Hybertsen, M. S.; Reichman, D. R.; Gao, J.; Zhu, X. Y., The quantum coherent mechanism for singlet fission: experiment and theory. *Acc Chem Res* **2013**, *46*, 1321-9.
(54) Akselrod, G. M.; Deotare, P. B.; Thompson, N. J.; Lee, J.; Tisdale, W. A.; Baldo, M. A.; Menon, V. M.; Bulović, V., Visualization of exciton transport in ordered and disordered molecular solids. *Nat Comm* **2014**, *5*, 3646.
(55) Rose, T. S.; Righini, R.; Fayer, M. D., Picosecond transient grating measurements of singlet exciton transport in anthracene single crystals. *Chem Phys Lett* **1984**, *106*, 13-19.
(56) Lloyd, S.; Mohseni, M., Symmetry-enhanced supertransfer of delocalized quantum states. *New J. Phys.* **2010**, *12*, 075020.
(57) Grisanti, L.; Olivier, Y.; Wang, L.; Athanasopoulos, S.; Cornil, J.; Beljonne, D., Roles of local and nonlocal electron-phonon couplings in triplet exciton diffusion in the anthracene crystal. *Phys. Rev. B* **2013**, *88*, 035450.
(58) Wilson, M. W.; Rao, A.; Johnson, K.; Gelinas, S.; di Pietro, R.; Clark, J.; Friend, R. H., Temperature-independent singlet exciton fission in tetracene. *J Am Chem Soc* **2013**, *135*, 16680-8.
(59) Fleming, G.; Millar, D.; Morris, G.; Morris, J.; Robinson, G., Exciton fission and annihilation in crystalline tetracene. *Australian Journal of Chemistry* **1977**, *30*, 2353-2359.
(60) Lukman, S.; Richter, J. M.; Yang, L.; Hu, P.; Wu, J.; Greenham, N. C.; Musser, A. J., Efficient singlet fission and triplet-pair emission in a family of zethrene diradicaloids. *J Am Chem Soc* **2017**, *139*, 18376-18385.
(61) Wan, Y.; Stradomska, A.; Fong, S.; Guo, Z.; Schaller, R. D.; Wiederrecht, G. P.; Knoester, J.; Huang, L., Exciton level structure and dynamics in tubular porphyrin aggregates. *J Phys Chem C* **2014**, *118*, 24854-24865.